Measurement of $e^+e^- \to \pi^+\pi^-\psi(2S)$ via initial state radiation at Belle

X. L. Wang,[60] C. Z. Yuan,[16] C. P. Shen,[2] P. Wang,[16] A. Abdesselam,[51] I. Adachi,[12,8] H. Aihara,[56] S. Al Said,[51,24] K. Arinstein,[3] D. M. Asner,[43] R. Ayad,[51] A. M. Bakich,[50] V. Bansal,[43] B. Bhuyan,[14] A. Bobrov,[3] G. Bonvicini,[61] M. Bračko,[30,21] T. E. Browder,[11] D. Červenkov,[4] P. Chang,[39] V. Chekelian,[31] A. Chen,[38] B. G. Cheon,[10] K. Chilikin,[20] R. Chistov,[20] K. Cho,[25] V. Chobanova,[31] S.-K. Choi,[9] Y. Choi,[49] D. Cinabro,[61] J. Dalseno,[31,53] M. Danilov,[20,33] Z. Doležal,[4] Z. Drásal,[4] A. Drutskoy,[20,33] K. Dutta,[14] S. Eidelman,[3] H. Farhat,[61] J. E. Fast,[43] T. Ferber,[6] V. Gaur,[52] A. Garmash,[3] D. Getzkow,[7] R. Gillard,[61] Y. M. Goh,[10] J. Haba,[12,8] K. Hayasaka,[36] H. Hayashii,[37] X. H. He,[44] W.-S. Hou,[39] T. Iijima,[36,35] K. Inami,[35] A. Ishikawa,[55] R. Itoh,[12,8] Y. Iwasaki,[12] D. Joffe,[23] T. Julius,[32] K. H. Kang,[27] E. Kato,[55] T. Kawasaki,[41] C. Kiesling,[31] D. Y. Kim,[48] H. J. Kim,[27] J. B. Kim,[26] J. H. Kim,[25] M. J. Kim,[27] S. H. Kim,[10] Y. J. Kim,[25] K. Kinoshita,[5] B. R. Ko,[26] P. Kodyš,[4] S. Korpar,[30,21] P. Križan,[64,21] P. Krokovny,[3] A. Kuzmin,[3] Y.-J. Kwon,[63] J. S. Lange,[7] I. S. Lee,[10] P. Lewis,[11] Y. Li,[60] L. Li Gioi,[31] J. Libby,[15] D. Liventsev,[12] P. Lukin,[3] D. Matvienko,[3] K. Miyabayashi,[37] H. Miyata,[41] R. Mizuk,[20,33] A. Moll,[31,53] T. Mori,[35] R. Mussa,[19] E. Nakano,[42] M. Nakao,[12,8] T. Nanut,[21] Z. Natkaniec,[40] N. K. Nisar,[52] S. Nishida,[12,8] S. Ogawa,[54] S. Okuno,[22] S. L. Olsen,[47] P. Pakhlov,[20,33] G. Pakhlova,[20] C. W. Park,[49] H. Park,[27] T. K. Pedlar,[29] R. Pestotnik,[21] M. Petrič,[21] L. E. Piilonen,[60] E. Ribežl,[21] M. Ritter,[31] A. Rostomyan,[6] S. Ryu,[47] Y. Sakai,[12,8] S. Sandilya,[52] L. Santelj,[21] T. Sanuki,[55] V. Savinov,[45] O. Schneider,[28] G. Schnell,[1,13] C. Schwanda,[17] D. Semmler,[7] K. Senyo,[62] V. Shebalin,[3] T.-A. Shibata,[57] J.-G. Shiu,[39] A. Sibidanov,[50] F. Simon,[31,53] Y.-S. Sohn,[63] A. Sokolov,[18] E. Solovieva,[20] M. Starič,[21] M. Steder,[6] T. Sumiyoshi,[58] U. Tamponi,[19,59] K. Tanida,[47] G. Tatishvili,[43] Y. Teramoto,[42] K. Trabelsi,[12,8] M. Uchida,[57] T. Uglov,[20,34] Y. Unno,[10] S. Uno,[12,8] Y. Usov,[3] C. Van Hulse,[1] P. Vanhoefer,[31] G. Varner,[11] A. Vinokurova,[3] M. N. Wagner,[7] Y. Watanabe,[22] E. Won,[26] S. Yashchenko,[6] Y. Yusa,[41] Z. P. Zhang,[46] V. Zhilich,[3] and A. Zupanc[21]

(Belle Collaboration)

[1]*University of the Basque Country UPV/EHU, 48080 Bilbao*
[2]*Beihang University, Beijing 100191*
[3]*Budker Institute of Nuclear Physics SB RAS and Novosibirsk State University, Novosibirsk 630090*
[4]*Faculty of Mathematics and Physics, Charles University, 121 16 Prague*
[5]*University of Cincinnati, Cincinnati, Ohio 45221*
[6]*Deutsches Elektronen–Synchrotron, 22607 Hamburg*
[7]*Justus-Liebig-Universität Gießen, 35392 Gießen*
[8]*The Graduate University for Advanced Studies, Hayama 240-0193*
[9]*Gyeongsang National University, Chinju 660-701*
[10]*Hanyang University, Seoul 133-791*
[11]*University of Hawaii, Honolulu, Hawaii 96822*
[12]*High Energy Accelerator Research Organization (KEK), Tsukuba 305-0801*
[13]*IKERBASQUE, Basque Foundation for Science, 48011 Bilbao*
[14]*Indian Institute of Technology Guwahati, Assam 781039*
[15]*Indian Institute of Technology Madras, Chennai 600036*
[16]*Institute of High Energy Physics, Chinese Academy of Sciences, Beijing 100049*
[17]*Institute of High Energy Physics, Vienna 1050*
[18]*Institute for High Energy Physics, Protvino 142281*
[19]*INFN - Sezione di Torino, 10125 Torino*
[20]*Institute for Theoretical and Experimental Physics, Moscow 117218*
[21]*J. Stefan Institute, 1000 Ljubljana*
[22]*Kanagawa University, Yokohama 221-8686*
[23]*Kennesaw State University, Kennesaw, Georgia 30144*
[24]*Department of Physics, Faculty of Science, King Abdulaziz University, Jeddah 21589*
[25]*Korea Institute of Science and Technology Information, Daejeon 305-806*
[26]*Korea University, Seoul 136-713*
[27]*Kyungpook National University, Daegu 702-701*
[28]*École Polytechnique Fédérale de Lausanne (EPFL), Lausanne 1015*
[29]*Luther College, Decorah, Iowa 52101*
[30]*University of Maribor, 2000 Maribor*
[31]*Max-Planck-Institut für Physik, 80805 München*
[32]*School of Physics, University of Melbourne, Victoria 3010*
[33]*Moscow Physical Engineering Institute, Moscow 115409*
[34]*Moscow Institute of Physics and Technology, Moscow Region 141700*

[35]*Graduate School of Science, Nagoya University, Nagoya 464-8602*
[36]*Kobayashi-Maskawa Institute, Nagoya University, Nagoya 464-8602*
[37]*Nara Women's University, Nara 630-8506*
[38]*National Central University, Chung-li 32054*
[39]*Department of Physics, National Taiwan University, Taipei 10617*
[40]*H. Niewodniczanski Institute of Nuclear Physics, Krakow 31-342*
[41]*Niigata University, Niigata 950-2181*
[42]*Osaka City University, Osaka 558-8585*
[43]*Pacific Northwest National Laboratory, Richland, Washington 99352*
[44]*Peking University, Beijing 100871*
[45]*University of Pittsburgh, Pittsburgh, Pennsylvania 15260*
[46]*University of Science and Technology of China, Hefei 230026*
[47]*Seoul National University, Seoul 151-742*
[48]*Soongsil University, Seoul 156-743*
[49]*Sungkyunkwan University, Suwon 440-746*
[50]*School of Physics, University of Sydney, New South Wales 2006*
[51]*Department of Physics, Faculty of Science, University of Tabuk, Tabuk 71451*
[52]*Tata Institute of Fundamental Research, Mumbai 400005*
[53]*Excellence Cluster Universe, Technische Universität München, 85748 Garching*
[54]*Toho University, Funabashi 274-8510*
[55]*Tohoku University, Sendai 980-8578*
[56]*Department of Physics, University of Tokyo, Tokyo 113-0033*
[57]*Tokyo Institute of Technology, Tokyo 152-8550*
[58]*Tokyo Metropolitan University, Tokyo 192-0397*
[59]*University of Torino, 10124 Torino*
[60]*CNP, Virginia Polytechnic Institute and State University, Blacksburg, Virginia 24061*
[61]*Wayne State University, Detroit, Michigan 48202*
[62]*Yamagata University, Yamagata 990-8560*
[63]*Yonsei University, Seoul 120-749*
[64]*Faculty of Mathematics and Physics, University of Ljubljana, 1000 Ljubljana*
(Received 28 October 2014; published 12 June 2015)

We report measurement of the cross section of $e^+e^- \to \pi^+\pi^-\psi(2S)$ between 4.0 and 5.5 GeV, based on an analysis of initial state radiation events in a 980 fb^{-1} data sample recorded with the Belle detector. The properties of the $Y(4360)$ and $Y(4660)$ states are determined. Fitting the mass spectrum of $\pi^+\pi^-\psi(2S)$ with two coherent Breit-Wigner functions, we find two solutions with identical mass and width but different couplings to electron-positron pairs: $M_{Y(4360)} = (4347 \pm 6 \pm 3)$ MeV/c^2, $\Gamma_{Y(4360)} = (103 \pm 9 \pm 5)$ MeV, $M_{Y(4660)} = (4652 \pm 10 \pm 8)$ MeV/c^2, $\Gamma_{Y(4660)} = (68 \pm 11 \pm 1)$ MeV; and $\mathcal{B}[Y(4360) \to \pi^+\pi^-\psi(2S)] \cdot \Gamma^{e^+e^-}_{Y(4360)} = (10.9 \pm 0.6 \pm 0.7)$ eV and $\mathcal{B}[Y(4660) \to \pi^+\pi^-\psi(2S)] \cdot \Gamma^{e^+e^-}_{Y(4660)} = (8.1 \pm 1.1 \pm 0.5)$ eV for one solution; or $\mathcal{B}[Y(4360) \to \pi^+\pi^-\psi(2S)] \cdot \Gamma^{e^+e^-}_{Y(4360)} = (9.2 \pm 0.6 \pm 0.6)$ eV and $\mathcal{B}[Y(4660) \to \pi^+\pi^-\psi(2S)] \cdot \Gamma^{e^+e^-}_{Y(4660)} = (2.0 \pm 0.3 \pm 0.2)$ eV for the other. Here, the first errors are statistical and the second systematic. Evidence for a charged charmoniumlike structure at 4.05 GeV/c^2 is observed in the $\pi^\pm\psi(2S)$ intermediate state in the $Y(4360)$ decays.

DOI: 10.1103/PhysRevD.91.112007 PACS numbers: 14.40.Pq, 13.25.Gv, 13.66.Bc

I. INTRODUCTION

Many charmonium and charmoniumlike states have been discovered in the past decade. Some are good candidates for conventional charmonium states, while others exhibit unusual properties consistent with expectations for exotic states such as tetraquarks, molecules, hybrids, hadrocharmonia, or glueballs [1,2]. The initial state radiation (ISR) technique has played a very important role in the discovery and studies of a number of the charmonium and charmoniumlike states. The J^{PC} quantum numbers of the final states accompanying the ISR photon(s) are restricted to $J^{PC} = 1^{--}$ and so favor this technique for the study of vector particles.

The *BABAR* experiment observed the $Y(4260)$ state in the process $e^+e^- \to \gamma_{ISR}\pi^+\pi^- J/\psi$ [3], and this was confirmed by the CLEO [4] and Belle experiments [5] with the same technique. Moreover, Belle reported a broad structure near 4.0 GeV that they dubbed the $Y(4008)$. In an analysis of the $e^+e^- \to \gamma_{ISR}\pi^+\pi^-\psi(2S)$ process, *BABAR* found a structure near 4.32 GeV [6], while Belle observed two

resonant structures at 4.36 and 4.66 GeV [7]. Recently, both *BABAR* and Belle updated their results on $e^+e^- \to \gamma_{\rm ISR}\pi^+\pi^- J/\psi$, which still show differences in the 4.008 GeV/c^2 mass region [8,9]; the latest $e^+e^- \to \gamma_{\rm ISR}\pi^+\pi^-\psi(2S)$ analysis from the *BABAR* experiment with its full data sample confirmed the existence of the $Y(4660)$ state [10]. However, in an ISR study of $e^+e^- \to \eta J/\psi$ by Belle, only the well-established $\psi(4040)$ and $\psi(4160)$ charmonium states, but no Y states, are observed [11]. A better understanding of the structures observed in these final states would benefit from improved measurements.

Complementary to the aforementioned neutral states, charged charmoniumlike structures were observed recently at Belle and BESIII in the $Y(4260) \to \pi^\mp Z(3900)^\pm \to \pi^+\pi^- J/\psi$ decays [9,12] and at BESIII in $e^+e^- \to \pi^\mp Z_c(4020)^\pm \to \pi^\mp(\pi^\pm h_c)$ [13]. Since these states contain both a $c\bar{c}$ component and electric charge, they are good candidates for tetraquark or meson molecular states. These or similar states may exist in the $\pi^\pm\psi(2S)$ invariant-mass distribution in the $e^+e^- \to \pi^+\pi^-\psi(2S)$ process.

To characterize more precisely the properties of the $Y(4360)$ and $Y(4660)$, to better understand their nature, and to search for possible charged charmoniumlike states decaying into $\pi^\pm\psi(2S)$, we measure the $e^+e^- \to \pi^+\pi^-\psi(2S)$ process using the ISR technique with the full Belle data that was collected with the Belle detector [14] at the KEKB asymmetric-energy e^+e^- collider (3.5 GeV e^+ and 8.0 GeV e^-) [15]. The results here for $Y(4360)$ and $Y(4660)$ supersede our previous measurements in Ref. [7].

In this analysis, $\psi(2S)$ is reconstructed in the $\pi^+\pi^- J/\psi$ (hereinafter denoted the "$\pi^+\pi^- J/\psi$ mode") and the $\mu^+\mu^-$ (the "$\mu^+\mu^-$ mode") final states and J/ψ is reconstructed in the $\ell^+\ell^-(\ell = e, \mu)$ final state. Due to the high background from Bhabha scattering, the $\psi(2S) \to e^+e^-$ decay is not used here. The 980 fb^{-1} data sample used for this analysis was collected at the $\Upsilon(nS)$ ($n = 1, 2, 3, 4$, or 5) resonances and center-of-mass energies a few tens of MeV lower than the $\Upsilon(4S)$ or the $\Upsilon(1S)/\Upsilon(2S)$ peaks.

II. DETECTOR AND MONTE CARLO SIMULATIONS

The Belle detector is a large-solid-angle magnetic spectrometer that consists of a silicon vertex detector, a 50-layer central drift chamber, an array of aerogel threshold Cherenkov counters, a barrel-like arrangement of time-of-flight scintillation counters, and an electromagnetic calorimeter comprised of CsI(Tl) crystals located inside a superconducting solenoid coil that provides a 1.5 T magnetic field. An iron flux return located outside of the coil is instrumented to detect $K^0_{\rm L}$ mesons and to identify muons. The origin of the coordinate system is defined as the position of the nominal interaction point. The z axis is aligned with the direction opposite the e^+ beam and is parallel to the direction of the magnetic field within the solenoid. The x axis is horizontal and points towards the outside of the storage ring and the y axis is vertical upward. The polar angle and azimuthal angle ϕ are measured relative to the positive z and x axes, respectively.

We use a GEANT-based Monte Carlo (MC) simulation [16] to model the response of the detector, identify potential backgrounds, and determine the acceptance. The MC simulation includes run-dependent detector performance variations and background conditions.

We use the event generator PHOKHARA [17] to simulate the process $e^+e^- \to \gamma_{\rm ISR} + Y$. In the generator, one or two ISR photons may be emitted before forming the resonance Y, which then decays to $\pi^+\pi^-\psi(2S)$, with $\psi(2S) \to \pi^+\pi^- J/\psi \to \pi^+\pi^-\ell^+\ell^-$ or $\psi(2S) \to \mu^+\mu^-$. The masses and widths of $Y(4360)$ and $Y(4660)$ determined in our previous measurement are used in the simulation [7].

III. EVENT SELECTION

For candidate events, we require six (four) well-reconstructed charged tracks with zero net charge for the $\psi(2S) \to \pi^+\pi^- J/\psi$ ($\psi(2S) \to \mu^+\mu^-$) mode. Well-reconstructed charged tracks have impact parameters perpendicular to and along the e^+ beam direction with respect to the interaction point that are less than 0.5 and 5.0 cm, respectively. The transverse momentum of each track is required to be greater than 0.1 GeV/c. For charged tracks, information from different detector subsystems is combined to form a likelihood $\mathcal{L}_i$ for particle species i [18]. Tracks with $\mathcal{R}_K = \mathcal{L}_K/(\mathcal{L}_K + \mathcal{L}_\pi) < 0.4$ are identified as pions with an efficiency of 95%; 6% of kaons are misidentified as pions. Similar likelihood ratios are formed for electron and muon identification [19,20]. For electrons from $J/\psi \to e^+e^-$, both tracks are required to have $\mathcal{R}_e > 0.1$. Bremsstrahlung photons detected in the electromagnetic calorimeter within 0.05 rad of the original lepton direction are included in the calculation of the $e^+e^-(\gamma)$ invariant mass. For muon candidates in the $\mu^+\mu^-$ mode, one of the tracks is required to have $\mathcal{R}_\mu > 0.9$ and the other track must have associated hits in the K_L-and-muon detector that agree with the extrapolated trajectory of a charged track found in the drift chamber. For muons in $J/\psi \to \mu^+\mu^-$, one track must have $\mathcal{R}_\mu > 0.9$, but no additional constraints are placed on the other track.

For the $\pi^+\pi^- J/\psi$ mode, there is a clear J/ψ signal in the lepton-pair invariant-mass distribution. Fitting the mass spectrum of the lepton pair with a Gaussian function and a linear background, we obtain an invariant mass of $M_{\ell^+\ell^-} = (3099.1 \pm 1.7)$ MeV/c^2 and a resolution ($\sigma_{\ell^+\ell^-}$) of (14.3 ± 1.3) MeV/c^2. The J/ψ signal region is defined as $m_{J/\psi} - 3\sigma_{\ell^+\ell^-} < M_{\ell^+\ell^-} < m_{J/\psi} + 3\sigma_{\ell^+\ell^-}$, where $m_{J/\psi}$ is the nominal world-average J/ψ mass [21]. In the 10% of events where there are multiple $\pi^+\pi^-$ combinations that satisfy the $\psi(2S)$ requirements, we select the one with $|M_{\pi^+\pi^-\ell^+\ell^-} - M_{\ell^+\ell^-}|$, the difference of the corresponding invariant masses, closest to the difference of the nominal

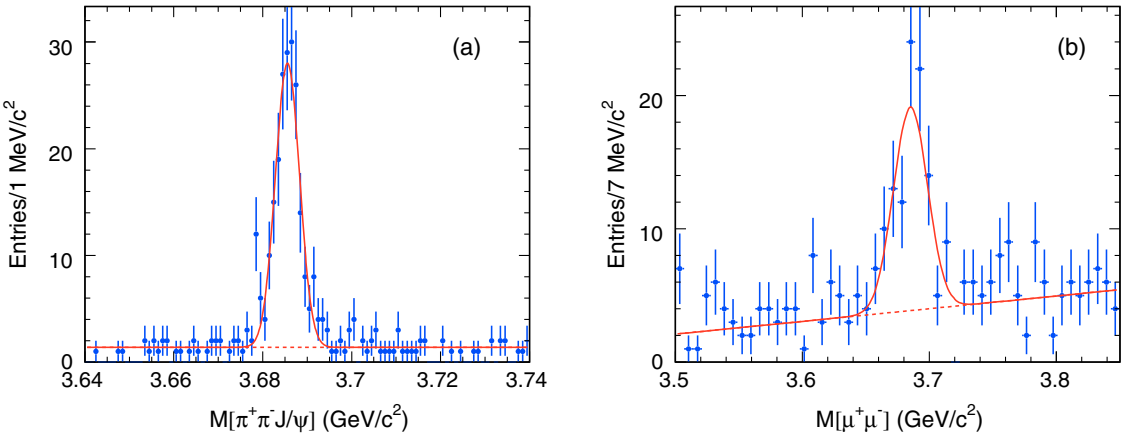

FIG. 1 (color online). Invariant-mass distributions of the candidate $\psi(2S)$ signals in (a) the $\pi^+\pi^- J/\psi$ mode and (b) the $\mu^+\mu^-$ mode. Dots with error bars are data and the curves are the best fits.

masses of $\psi(2S)$ and J/ψ. Fitting the mass spectrum of the candidate $\pi^+\pi^- J/\psi$-mode events [22] with a Gaussian function and a linear background, shown in Fig. 1(a), we obtain an invariant mass of (3685.4 ± 0.2) MeV/c^2 with a resolution of (2.7 ± 0.2) MeV/c^2. The $\psi(2S)$ sample is nearly background free. The $\psi(2S)$ signal region is defined as 3.67 GeV/$c^2 < M_{\pi^+\pi^- J/\psi} < 3.70$ GeV/c^2, as in our previous measurement [7]. The sideband regions are defined as 3.64 GeV/$c^2 < M_{\pi^+\pi^- J/\psi} < 3.67$ GeV/c^2 and 3.70 GeV/$c^2 < M_{\pi^+\pi^- J/\psi} < 3.73$ GeV/c^2, double the width of the signal region.

For the $\mu^+\mu^-$ mode, the invariant-mass distribution of the $\mu^+\mu^-$ pair ($M_{\mu^+\mu^-}$) shows a clear $\psi(2S)$ signal. From the fit, shown in Fig. 1(b), we obtain an invariant mass of (3685.2 ± 2.5) MeV/c^2 with a resolution of (13.8 ± 2.0) MeV/c^2. The $\psi(2S)$ signal region is defined as 3.651 GeV/$c^2 < M_{\mu^+\mu^-} < 3.721$ GeV/c^2. The sideband regions are defined as 3.5215 GeV/$c^2 < M_{\mu^+\mu^-} < 3.6265$ GeV/c^2 and 3.7455 GeV/$c^2 < M_{\mu^+\mu^-} < 3.8505$ GeV/c^2, triple the width of the signal region.

For both modes, some γ conversions are misidentified as $\pi^+\pi^-$; these events are removed by requiring $\mathcal{R}_e < 0.75$ for

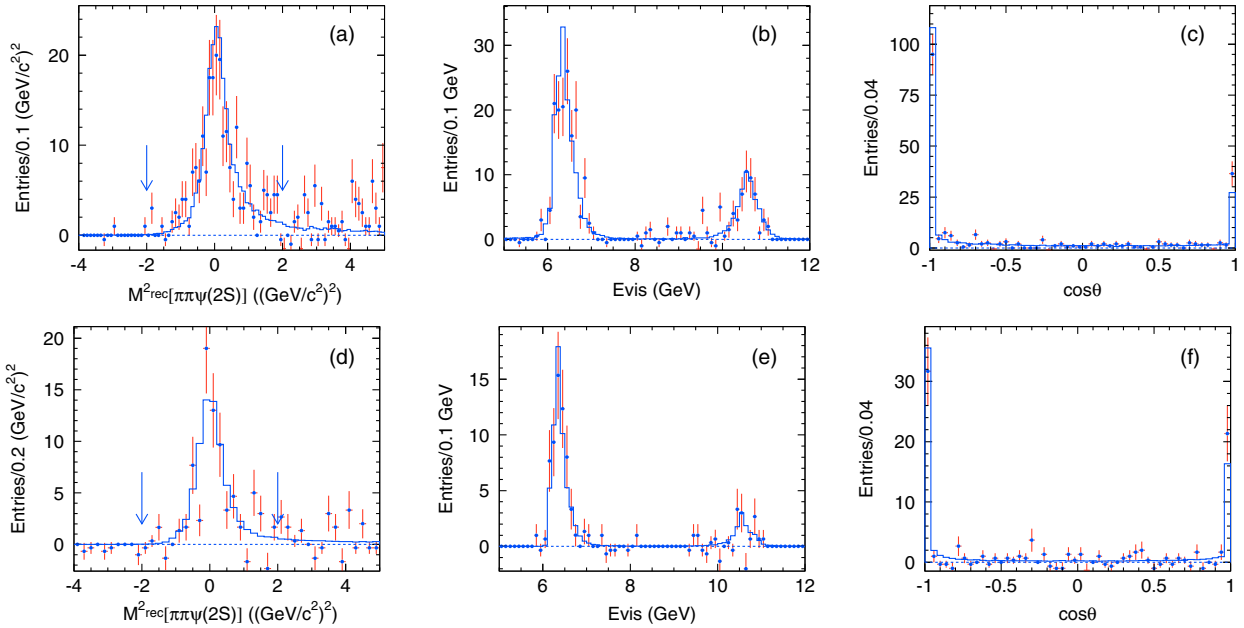

FIG. 2 (color online). The ISR characteristics of the selected events. The first row is for the $\pi^+\pi^- J/\psi$ mode and the second for the $\mu^+\mu^-$ mode. Panels (a) and (d) show the square of the mass recoiling against the $\pi^+\pi^-\psi(2S)$ system; (b) and (e) show the visible energy in the detector; (c) and (f) show the polar-angle distribution of the $\pi^+\pi^-\psi(2S)$ system in the e^+e^- center-of-mass frame. Points with error bars (histograms) represent the data (MC simulation, described in Sec. I). The backgrounds, estimated from the normalized $\psi(2S)$ mass sidebands, have been subtracted from the distributions.

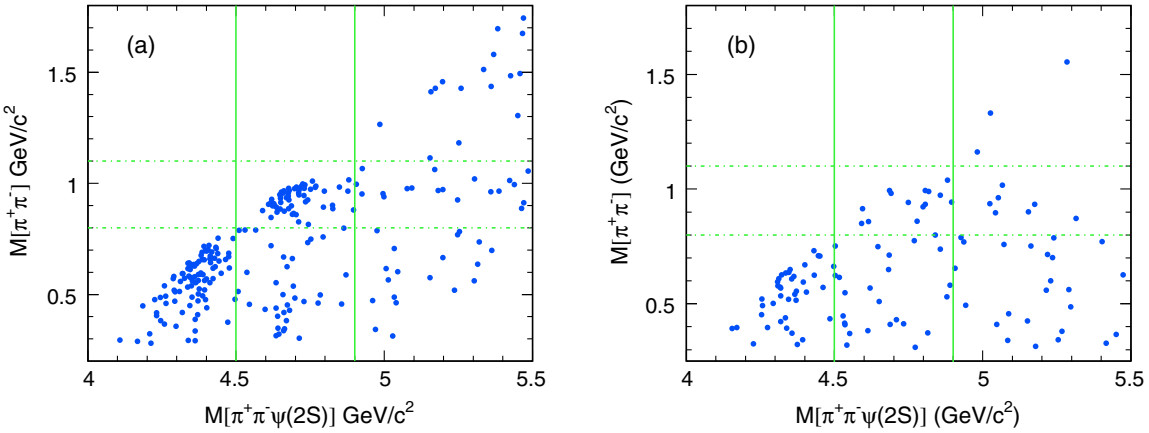

FIG. 3 (color online). Invariant mass of the $\pi^+\pi^-$ recoiling against the $\psi(2S)$ versus the invariant mass of the $\pi^+\pi^-\psi(2S)$ in the $\pi^+\pi^- J/\psi$ mode (a) and $\mu^+\mu^-$ mode (b). The horizontal dashed lines show the belt of $f_0(980)$, while the vertical solid lines demarcate the regions with the $Y(4360)$ and $Y(4660)$ states and the higher-mass combinations.

the π^+ and π^- daughters of the $\psi(2S)$. This background is worse in the $\mu^+\mu^-$ mode and so an invariant mass $M_{\pi^+\pi^-} > 0.31$ GeV/c^2 is also required.

The detection of the ISR photon ($\gamma_{\rm ISR}$) is optional; instead, we require $-2.0\,({\rm GeV}/c^2)^2 < M^2_{\rm rec} < 2.0\,({\rm GeV}/c^2)^2$, where $M^2_{\rm rec}$ is the square of the mass recoiling against the $\pi^+\pi^-\psi(2S)$ system. Good agreement between data and MC simulation for the visible energy ($E_{\rm vis}$) and polar-angle distributions of the $\pi^+\pi^-\psi(2S)$ system in the e^+e^- center-of-mass frame confirms that the signal events are produced via ISR. Here, $E_{\rm vis}$ encompasses all final-state photons and charged particles; energies for the latter are calculated from track momenta, assuming the tracks to be pions. The distributions of $M^2_{\rm rec}$, $E_{\rm vis}$, and polar-angle distributions of the $\pi^+\pi^- J/\psi$ and $\mu^+\mu^-$ modes are shown in Fig. 2.

After all the above selections, there are 245 $\pi^+\pi^-\psi(2S)$ candidate events with 28 background events in the $\pi^+\pi^- J/\psi$ mode, and 118 candidate events with 56 background events in the $\mu^+\mu^-$ mode; the background yields are estimated from the corresponding sidebands. Figure 3 shows the scatter plots of the invariant mass $M_{\pi^+\pi^-}$ of the $\pi^+\pi^-$ pair recoiling against the $\psi(2S)$ versus the invariant mass $M_{\pi^+\pi^-\psi(2S)}$ of the $\pi^+\pi^-\psi(2S)$ combination [23]. The corresponding distribution of the candidate events in the $\mu^+\mu^-$ mode is similar but with lower statistics. There are two clusters of events corresponding to the $Y(4360)$ and $Y(4660)$. The $M_{\pi^+\pi^-}$ distributions tend to cluster around the masses of $f_0(500)$ and $f_0(980)$. Figure 4 shows the projection onto the $M_{\pi^+\pi^-}$ axis in the cleaner $\pi^+\pi^- J/\psi$ mode, compared with MC simulation that assumes an incoherent sum of the $f_0(500)$ and $f_0(980)$. Additionally, the angular distributions of $\pi^\pm$ and $\pi^+\pi^-$ pair are compared. Figure 5 shows the angular distributions of π in the $\pi^+\pi^-$ system, and Fig. 6 shows the $\pi^+\pi^-$ in $\pi^+\pi^-\psi(2S)$ system. The data are from the clean $\pi^+\pi^- J/\psi$ mode, and the MC simulations are generated assuming S-wave between π^+ and π^- in $\pi^+\pi^-$ system and S-wave between $\pi^+\pi^-$ and $\psi(2S)$ in $\pi^+\pi^-\psi(2S)$ system.

IV. FIT TO $M_{\pi^+\pi^-\psi(2S)}$ AND MEASUREMENT OF CROSS SECTIONS

Figure 9 shows the $M_{\pi^+\pi^-\psi(2S)}$ distributions in the $\pi^+\pi^- J/\psi$ and $\mu^+\mu^-$ modes; the structures in these two

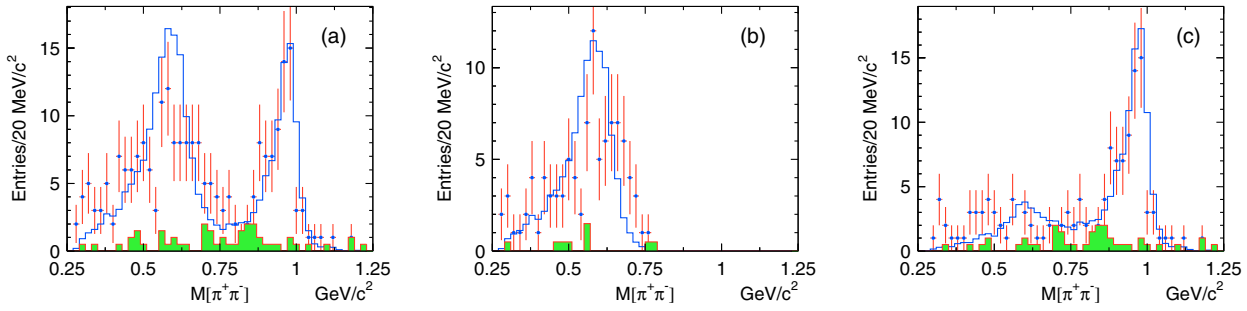

FIG. 4 (color online). Invariant-mass distributions of $\pi^+\pi^-$ from $Y(4360)$ and $Y(4660)$ decays in the $\pi^+\pi^- J/\psi$ mode. Points with error bars (open histograms) represent the data (MC simulation, described in Sec. I); the shaded histograms represent the background estimated from the scaled sidebands. Panel (a) is for the events in the region 4.0 GeV/c^2 < $M_{\pi^+\pi^-\psi(2S)}$ < 5.5 GeV/c^2, (b) for events in the $Y(4360)$ region (4.0 to 4.5 GeV/c^2), and (c) for the events in $Y(4660)$ region (4.5 to 5.5 GeV/c^2).

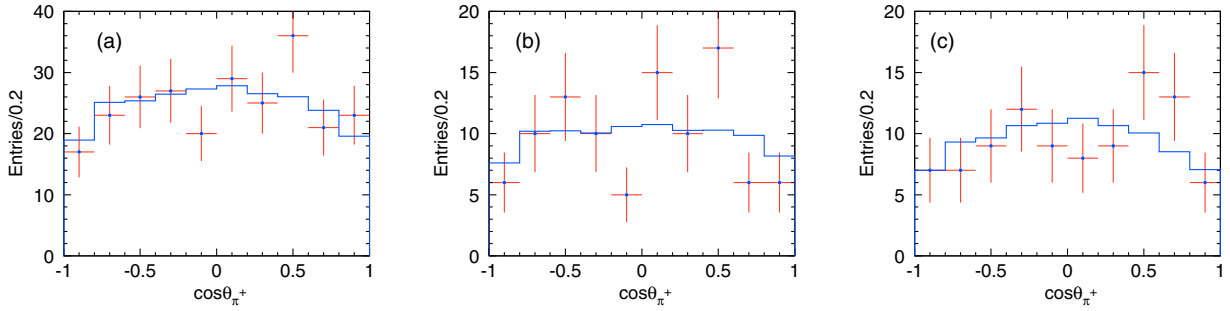

FIG. 5 (color online). Angular distributions of π in the $\pi^+\pi^-$ system in $\pi^+\pi^- J/\psi$ mode. Panel (a) is for the events in the region 4.0 GeV/c^2 < $M_{\pi^+\pi^-\psi(2S)}$ < 5.5 GeV/c^2, (b) for events in the $Y(4360)$ region (4.0 to 4.5 GeV/c^2), and (c) for the events in $Y(4660)$ region (4.5 to 4.9 GeV/c^2). The dots with error bars are data and the histograms are from MC simulation.

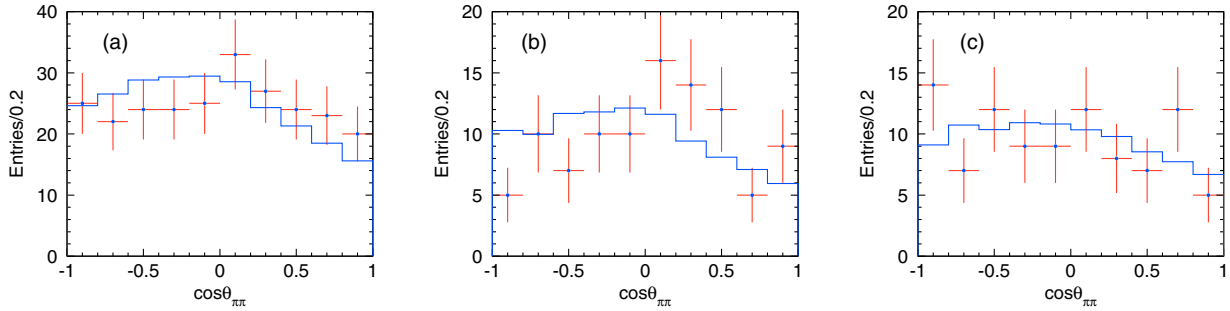

FIG. 6 (color online). Angular distributions of the $\pi^+\pi^-$ in $\pi^+\pi^-\psi(2S)$ system in the $\pi^+\pi^- J/\psi$ mode. Panel (a) is for the events in the region 4.0 GeV/c^2 < $M_{\pi^+\pi^-\psi(2S)}$ < 5.5 GeV/c^2, (b) for events in the $Y(4360)$ region (4.0 to 4.5 GeV/c^2), and (c) for the events in $Y(4660)$ region (4.5 to 4.9 GeV/c^2). The dots with error bars are data, while the histograms are MC simulation.

modes agree with each other within statistics. To extract the resonant parameters of the two Y states, an unbinned maximum-likelihood fit is performed to the mass spectra $M_{\pi^+\pi^-\psi(2S)} \in [4.0, 5.5]$ GeV/c^2 simultaneously for the $\pi^+\pi^- J/\psi$ and $\mu^+\mu^-$ modes, assuming that only two resonances and an incoherent featureless background contribute. The $\psi(2S)$ mass sidebands are included in the fit to estimate the backgrounds in the signal region; here, the fit assumes only the background component. The fit to the events in the signal region includes two coherent P-wave Breit-Wigner functions, f_1 for the $Y(4360)$ and f_2 for the $Y(4660)$.

The amplitude of the Breit-Wigner function f_j $(j = 1, 2)$ is defined as

$$f_j(M_{\pi^+\pi^-\psi(2S)}) = \frac{M_j}{M_{\pi^+\pi^-\psi(2S)}} \frac{\sqrt{12\pi\mathcal{B}_j(\pi^+\pi^-\psi(2S))\Gamma_j^{e^+e^-}\Gamma_j}}{M^2_{\pi^+\pi^-\psi(2S)} - M_j^2 + iM_j\Gamma_j} \cdot \sqrt{\frac{\Phi(M_{\pi^+\pi^-\psi(2S)})}{\Phi(M_j)}}, \quad (1)$$

where $\Gamma_j^{e^+e^-}$ is the partial width to e^+e^-, Γ_j the total width that is assumed to be a constant, and $\mathcal{B}_j(\pi^+\pi^-\psi(2S))$ the branching fraction of the resonance's decay to $\pi^+\pi^-\psi(2S)$. $\Phi(m)$ is the three-body phase-space factor for a resonance of mass m that decays to $\pi^+\pi^-\psi(2S)$. In the fit, M_j, Γ_j, and the product $\mathcal{B}_j(\pi^+\pi^-\psi(2S))\Gamma_j^{e^+e^-}$ are free parameters.

The signal amplitude is $A = f_1 + f_2 \cdot e^{i\phi}$, where ϕ is the relative phase between the two resonances, and the $M_{\pi^+\pi^-\psi(2S)}$ distribution of signal events is then $\mathcal{L}_{\rm eff} \cdot \varepsilon \cdot |A|^2$. Here the $\mathcal{L}_{\rm eff}$ is the effective luminosity and ε is the $M_{\pi^+\pi^-\psi(2S)}$-dependent efficiency. The effective luminosity of ISR is calculated according to theoretical formulas [24] and the integrated luminosity of Belle data, which is shown in Fig. 7. To determine the efficiency in the

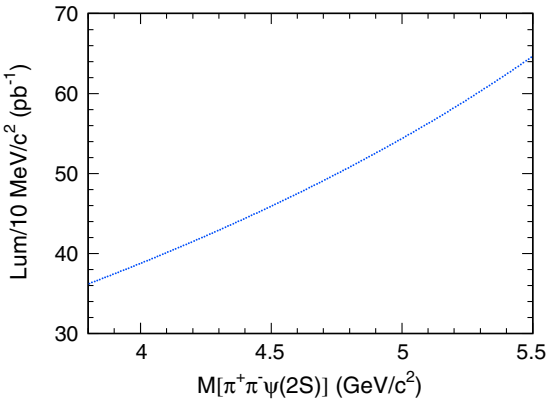

FIG. 7 (color online). The effective luminosity of ISR production with the full data sample.

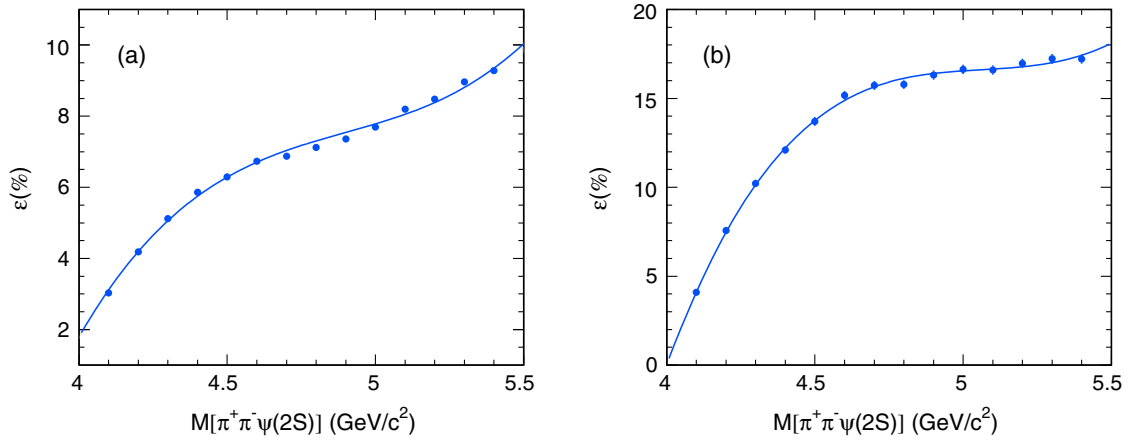

FIG. 8 (color online). The efficiency curves and the fit to third-order polynomials. Plot (a) is $\pi^+\pi^- J/\psi$ mode, and (b) is $\mu^+\mu^-$ mode.

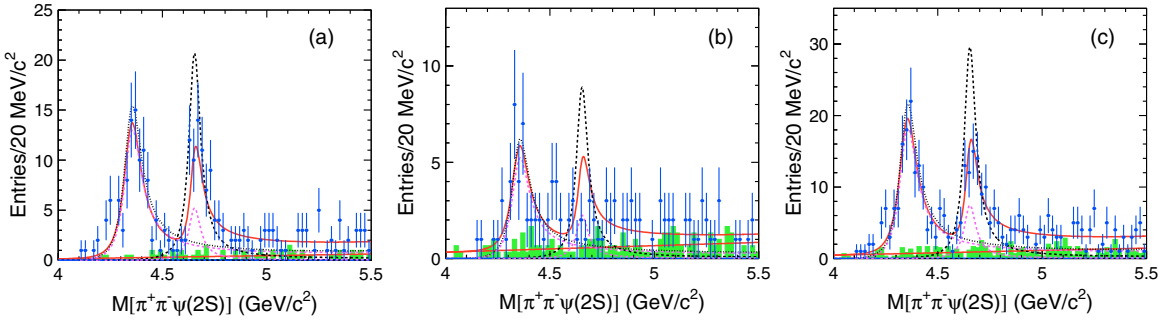

FIG. 9 (color online). The $\pi^+\pi^-\psi(2S)$ invariant-mass distributions and the simultaneous fit results described in the text. From left to right: (a) the $\pi^+\pi^- J/\psi$ mode, (b) the $\mu^+\mu^-$ mode, and (c) the sum. The points with error bars show the data while the shaded histograms are the scaled sideband backgrounds. The solid red curves show the best fits; the dashed curves, which are from the two fit solutions, show the contributions from the two Breit-Wigner components (described in the text). The interference between the two resonances is not shown.

range of $4.0\ \mathrm{GeV}/c^2 < M_{\pi^+\pi^-\psi(2S)} < 5.5\ \mathrm{GeV}/c^2$, MC samples with different $M_{\pi^+\pi^-\psi(2S)}$ are generated and simulated. The efficiency curves are shown in Fig. 8. The mass resolution, which is determined from MC simulation to range from 2 to 5 MeV/c^2 over the fit region, is small compared with the widths of the observed structures, and so is neglected. The fit results are shown in Fig. 9 and Tables I and II. There are two solutions with equally good fit quality; the χ^2/ndf is 18.7/21, where ndf is the number of degrees of freedom.

Since there are a number of events in the vicinity of the $Y(4260)$ mass, an alternative fit with a coherent sum of $Y(4260)$, $Y(4360)$, and $Y(4660)$ amplitudes is performed. In this fit, the mass and total width of the $Y(4260)$ state are

TABLE I. Results of the fits to the $\pi^+\pi^-\psi(2S)$ invariant-mass spectra. The first error is statistical and the second systematic. M, Γ, and $\mathcal{B}\cdot\Gamma^{e^+e^-}$ are the mass (in MeV/c^2), total width (in MeV), and the product of the branching fraction to $\pi^+\pi^-\psi(2S)$ and the e^+e^- partial width (in eV), respectively; ϕ is the relative phase between the two resonances (in degrees).

Parameters	Solution I	Solution II
$M_{Y(4360)}$	$4347 \pm 6 \pm 3$	
$\Gamma_{Y(4360)}$	$103 \pm 9 \pm 5$	
$\mathcal{B}[Y(4360) \to \pi^+\pi^-\psi(2S)] \cdot \Gamma^{e^+e^-}_{Y(4360)}$	$9.2 \pm 0.6 \pm 0.6$	$10.9 \pm 0.6 \pm 0.7$
$M_{Y(4660)}$	$4652 \pm 10 \pm 11$	
$\Gamma_{Y(4660)}$	$68 \pm 11 \pm 5$	
$\mathcal{B}[Y(4660) \to \pi^+\pi^-\psi(2S)] \cdot \Gamma^{e^+e^-}_{Y(4660)}$	$2.0 \pm 0.3 \pm 0.2$	$8.1 \pm 1.1 \pm 1.0$
ϕ	$32 \pm 18 \pm 20$	$272 \pm 8 \pm 7$

TABLE II. The correlations between the fit parameters shown in Table I (with the units given there). The numbers in parentheses are for the second solution.

	$\Gamma_{Y(4360)}$	$\mathcal{B}\cdot\Gamma^{e^+e^-}_{Y(4360)}$	$M_{Y(4660)}$	$\Gamma_{Y(4660)}$	$\mathcal{B}\cdot\Gamma^{e^+e^-}_{Y(4660)}$	ϕ
$M_{Y(4360)}$	−0.34 (−0.34)	0.04 (0.04)	−0.29 (−0.29)	0.05 (0.05)	0.30 (−0.13)	−0.37 (0.36)
$\Gamma_{Y(4360)}$	1.00	0.12 (0.12)	−0.08 (−0.08)	−0.28 (−0.28)	−0.45 (−0.11)	−0.08 (−0.10)
$\mathcal{B}\cdot\Gamma^{e^+e^-}_{Y(4360)}$		1.00	−0.37 (−0.22)	−0.32 (0.01)	−0.28 (0.03)	−0.40 (0.06)
$M_{Y(4660)}$			1.00	0.21 (0.21)	−0.06 (0.54)	0.86 (−0.76)
$\Gamma_{Y(4660)}$				1.00	0.14 (0.74)	0.25 (−0.44)
$\mathcal{B}\cdot\Gamma^{e^+e^-}_{Y(4660)}$					1.00	−0.17 (−0.72)

fixed to their latest measured values [9]. There are four solutions with equally good fit quality: $\chi^2/\mathrm{ndf} = 14.8/19$. The signal significance of the $Y(4260)$ is estimated to be 2.4σ by comparing the likelihood difference when the $Y(4260)$ is included in or excluded from the fit. The fit results are shown in Fig. 10 and Table III. Since this significance is marginal, the solutions without $Y(4260)$ are taken as the nominal results.

To compare with our previous measurement [7], the fit to the $\pi^+\pi^- J/\psi$ mode alone is performed. The differences can be explained by the strong correlation between the parameters (see Table II). For this mode alone, we also compare the alternative fit including the $Y(4260)$ with the nominal fit and consistent results with a 2.8σ statistical significance for the $Y(4260)$ signal. The results are discussed further in Appendix A.

The invariant-mass distributions of the two modes are combined together. The cross section for $e^+e^- \to \pi^+\pi^-\psi(2S)$ in each $\pi^+\pi^-\psi(2S)$ mass bin is calculated according to

$$\sigma_i = \frac{n_i^{\mathrm{obs}} - n_i^{\mathrm{bkg}}}{\mathcal{L}_i \sum_{j=1}^{2} \varepsilon_{ij}\mathcal{B}_j},$$

where j identifies the decay mode of $\psi(2S)$ ($j = 1$ for the $\pi^+\pi^- J/\psi$ mode and $j = 2$ for the $\mu^+\mu^-$ mode) and i indicates the mass bin; n_i^{obs}, n_i^{bkg}, ε_{ij}, $\mathcal{L}_i$, and $\mathcal{B}_j$ are the

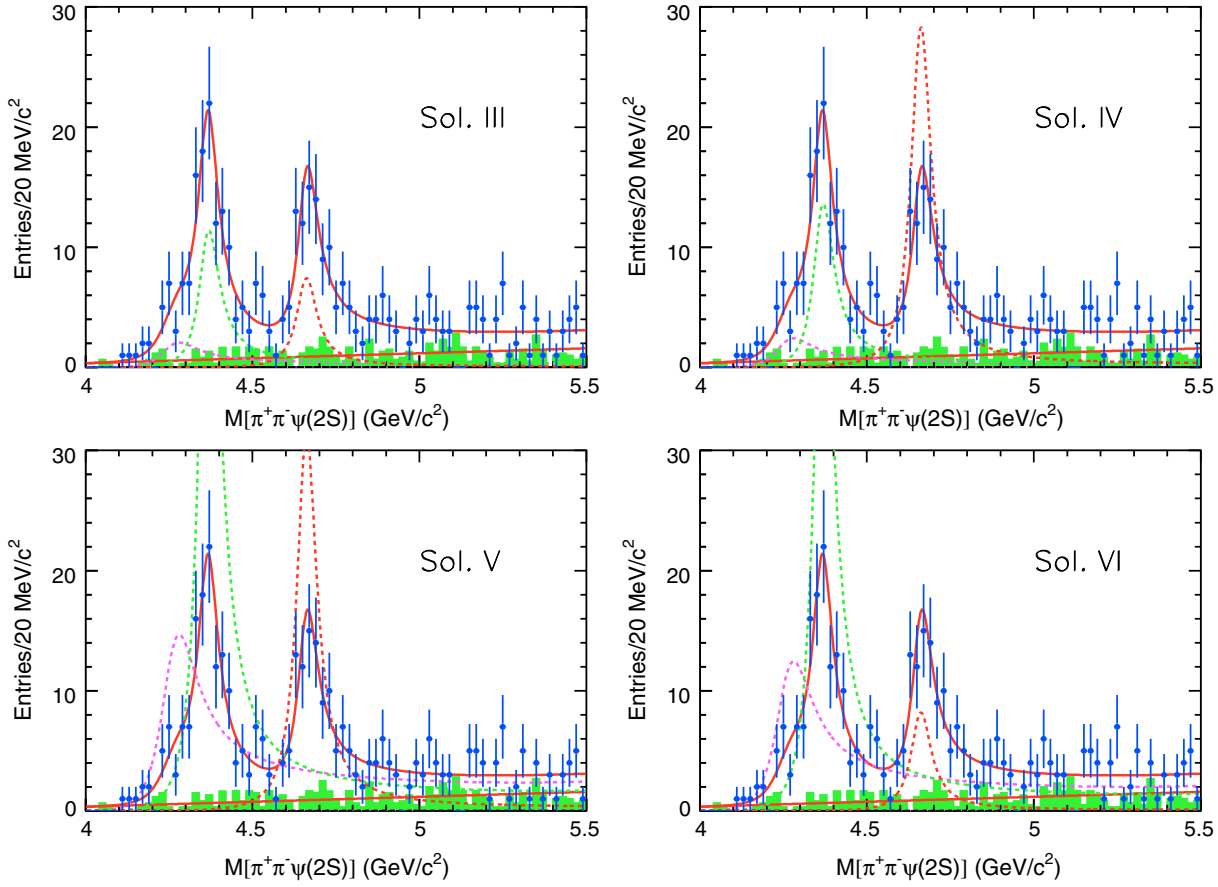

FIG. 10 (color online). The four solutions from the fit to the $\pi^+\pi^-\psi(2S)$ invariant-mass spectra with the $Y(4260)$ included. The curves show the best fit and the dashed curves show the contributions from the three Breit-Wigner components.

TABLE III. Results of the alternative fits to the $\pi^+\pi^-\psi(2S)$ invariant-mass spectra using three resonances: $Y(4260)$, $Y(4360)$, and $Y(4660)$. The parameters are the same as in Table I, except that, here, ϕ_1 is the relative phase between the $Y(4360)$ and $Y(4260)$ (in degrees) and ϕ_2 is the relative phase between the $Y(4360)$ and $Y(4660)$ (in degrees).

Parameters	Solution III	Solution IV	Solution V	Solution VI
$M_{Y(4260)}$		4259 (fixed)		
$\Gamma_{Y(4260)}$		134 (fixed)		
$\mathcal{B}[Y(4260) \to \pi^+\pi^-\psi(2S)] \cdot \Gamma^{e^+e^-}_{Y(4260)}$	$1.5 \pm 0.6 \pm 0.4$	$1.7 \pm 0.7 \pm 0.5$	$10.4 \pm 1.3 \pm 0.8$	$8.9 \pm 1.2 \pm 0.8$
$M_{Y(4360)}$		$4365 \pm 7 \pm 4$		
$\Gamma_{Y(4360)}$		$74 \pm 14 \pm 4$		
$\mathcal{B}[Y(4360) \to \pi^+\pi^-\psi(2S)] \cdot \Gamma^{e^+e^-}_{Y(4360)}$	$4.1 \pm 1.0 \pm 0.6$	$4.9 \pm 1.3 \pm 0.6$	$21.1 \pm 3.5 \pm 1.4$	$17.7 \pm 2.6 \pm 1.5$
$M_{Y(4660)}$		$4660 \pm 9 \pm 12$		
$\Gamma_{Y(4660)}$		$74 \pm 12 \pm 4$		
$\mathcal{B}[Y(4660) \to \pi^+\pi^-\psi(2S)] \cdot \Gamma^{e^+e^-}_{Y(4660)}$	$2.2 \pm 0.4 \pm 0.2$	$8.4 \pm 0.9 \pm 0.9$	$9.3 \pm 1.2 \pm 1.0$	$2.4 \pm 0.5 \pm 0.3$
ϕ_1	$304 \pm 24 \pm 21$	$294 \pm 25 \pm 23$	$130 \pm 4 \pm 2$	$141 \pm 5 \pm 4$
ϕ_2	$26 \pm 19 \pm 10$	$238 \pm 14 \pm 21$	$329 \pm 8 \pm 5$	$117 \pm 23 \pm 25$

number of events observed in data, the number of background events estimated from the fit to the events in the sidebands and scaled to the signal region, the detection efficiency of the jth mode, the effective luminosity in the ith $\pi^+\pi^-\psi(2S)$ mass bin, and the branching fractions of the jth mode [21], respectively. The resulting cross sections in the full solid angle are shown in Fig. 11 and Appendix B, where the error bars include statistical uncertainties in the signal and the subtracted background and all the systematic errors. The systematic error for the cross-section measurement is 4.8% and is the same for all data points.

V. SYSTEMATIC ERRORS

The systematic uncertainties in the cross-section measurements are summarized in Table IV and discussed below.

The particle identification uncertainty is 3.3% for the $\pi^+\pi^-J/\psi$ mode and 1.4% for the $\mu^+\mu^-$ mode. The uncertainty in the tracking efficiency is 0.35% per track and is additive. The efficiency differences between data and MC due to the corresponding resolutions in the J/ψ mass, $\psi(2S)$ mass, and $M^2_{\rm rec}$ requirements are measured with the control sample $e^+e^- \to \psi(2S) \to \pi^+\pi^-J/\psi$ [9]. The MC efficiency is found to be higher than in data by $(4.3 \pm 0.7)\%$ for the $\pi^+\pi^-J/\psi$ mode and $(4.4 \pm 0.3)\%$ for the $\mu^+\mu^-$ mode. A correction factor of 1.043 (1.044) is applied to the $\pi^+\pi^-J/\psi$ ($\mu^+\mu^-$) mode, leaving 0.7% (0.3%) as the residual systematic error.

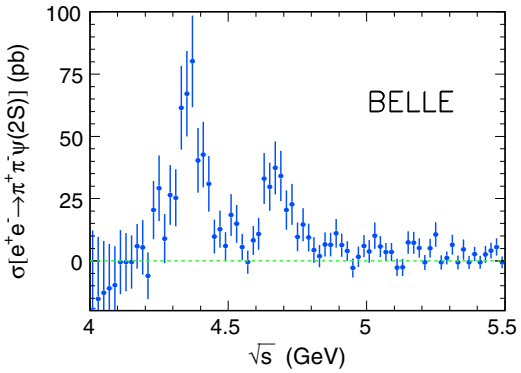

FIG. 11 (color online). The measured $e^+e^- \to \pi^+\pi^-\psi(2S)$ cross section for $\sqrt{s} = 4.0$ to 5.5 GeV. The errors are the sum in quadrature of the summed statistical errors of the numbers of signal and background events and the systematic errors.

The luminosity uncertainty of 1.4% is due mainly to the uncertainty from the Bhabha generator. The trigger efficiency for the events surviving the selection criteria is $(98.7 \pm 0.1(\text{stat}))\%$ for the $\pi^+\pi^-J/\psi$ mode and $(91.4 \pm 0.6(\text{stat}))\%$ for the $\mu^+\mu^-$ mode, based on the trigger simulation. A value of 1.0% is taken as a conservative estimate of the systematic error for the $\pi^+\pi^-J/\psi$ mode; 1.5% is used for the $\mu^+\mu^-$ mode.

Uncertainties in the simulation of the ISR process with PHOKHARA contributes less than 1.0%, and the largest uncertainty in the MC generation of signal events is from the simulation of the $M_{\pi^+\pi^-}$ from Y decays. We generate another MC sample with $m_{f_0(500)} = 0.7$ GeV/c^2 and $\Gamma_{f_0(500)} = 0.2$ GeV in order to check the efficiency variation. The efficiency changes by 2.0% at 4.4 GeV/c^2 and 3.8% at 4.7 GeV/c^2; half of the larger efficiency difference, 1.9%, is taken as the systematic error. The possible existence of the Z_c structure in $\pi^\pm\psi(2S)$ system does not affect the efficiency significantly and is thus neglected.

The uncertainties in the intermediate decay branching fractions taken from Ref. [21] contribute systematic errors of 1.0% for the $\pi^+\pi^-J/\psi$ mode and 10.4% for the $\mu^+\mu^-$ mode. The statistical error in the MC determination of the efficiency is less than 0.1%.

Assuming all the sources are independent and adding them in quadrature, we obtain total systematic errors in the cross-section measurement of 5.0% for the $\pi^+\pi^-J/\psi$ mode and

11.0% for the $\mu^+\mu^-$ mode. The combined systematic error of the two modes is 4.8%, when the correlations from particle ID, tracking, luminosity, and generator are considered.

To estimate the errors in $\mathcal{B}\cdot\Gamma^{e^+e^-}$, the uncertainties from the parametrization of the resonances, the phase-space factor due to the intermediate state in $M_{\pi^+\pi^-}$ in $Y(4660)$ decays, the fit range, and the background shape are also considered, in addition to those in the cross-section measurement. If a charged structure in $\pi^\pm\psi(2S)$ exists (cf. Sec. VI), it may affect the determination of the resonant parameters. A test fit to $\pi^+\pi^-\psi(2S)$ invariant-mass spectra is tried. Two components of $Y(4360)$ decays are included in the fit, one decaying to $\pi^+\pi^-\psi(2S)$ according to three-body phase space (50%) and the other decaying to $\pi^\pm Z_c^\mp$ (50%). Since the statistical errors of Z_c mass and width are large, the mass is fixed to be 4.05 GeV/c^2 when the two-body phase space is calculated. No Z_c substructure is included in $Y(4660)$ decays. Fit with either $Y(4360)+Y(4660)$ or $Y(4260)+Y(4360)+Y(4660)$ does not result in significant change in the resonant parameters of the $Y(4360)$ and $Y(4660)$. Since the charged structure is not significant (cf. Sec. VI), the effect due to possible existence of the Z_c states is not considered. The factor $M_i/M(\pi^+\pi^-\psi(2S))$ in Eq. (1) is removed in the fit when estimating the uncertainties from resonance parametrization. Half of the difference on each fit result with and without this factor is taken as the systematic error of resonance parametrization. In addition, systematic-error contributions are determined when the fit range is changed from $[4.0, 5.5]$ GeV/c^2 to $[4.0, 5.3]$ GeV/c^2 and, separately, the background shape is changed from a first-order polynomial to a constant.

TABLE IV. Relative systematic errors (in %) in the $\pi^+\pi^-\psi(2S)$ production cross-section measurement.

Source	$\pi^+\pi^- J/\psi$ mode	$\mu^+\mu^-$ mode	Common
Particle ID	3.3	1.4	1.4
Tracking	2.1	1.4	2.1
J/ψ, $\psi(2S)$ mass and $M^2_{\rm rec}$	0.7	0.3	···
Luminosity	1.4	1.4	1.4
Generator	1.9	1.9	1.9
Trigger	1.0	1.5	···
Branching fractions	1.6	10.4	···
MC statistics	0.1	0.1	···
Sum in quadrature	4.99	10.95	3.46
Sum of the two modes		4.8	

VI. INTERMEDIATE STATES

We search for charged charmoniumlike structures in both $\psi(2S)$ decay modes of the $\pi^\pm\psi(2S)$ system from

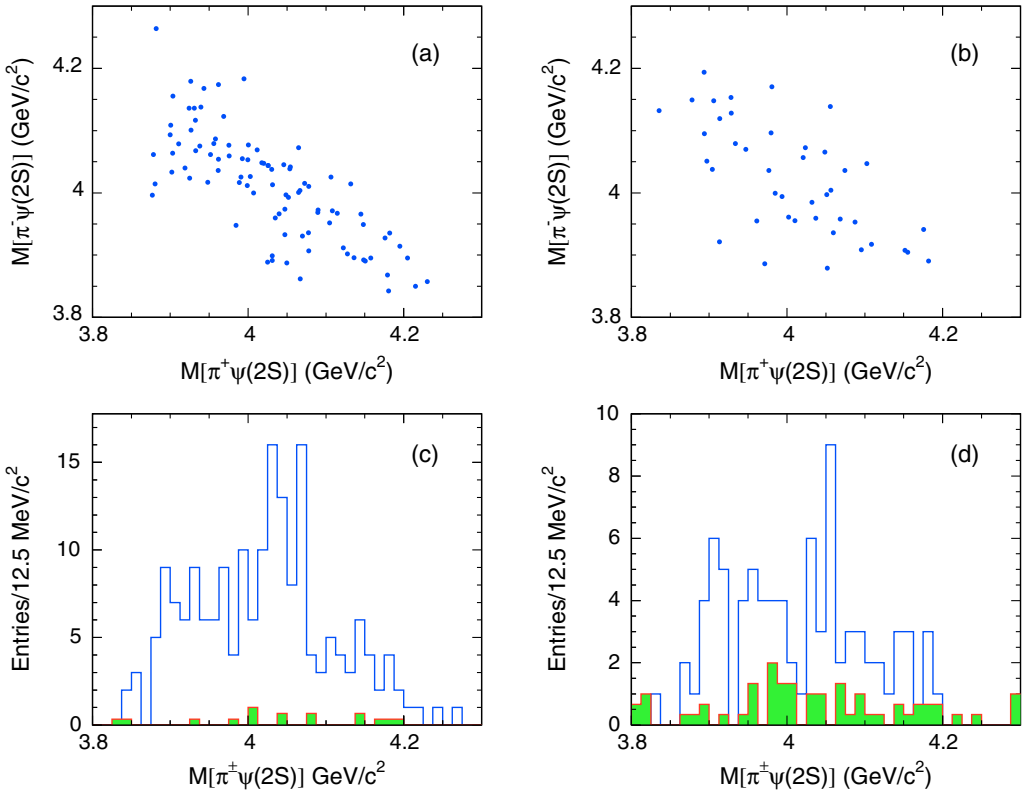

FIG. 12 (color online). The scatter plots of $M_{\pi^-\psi(2S)}$ versus $M_{\pi^+\psi(2S)}$ for the $Y(4360)$-subsample events in (a) the $\pi^+\pi^- J/\psi$ mode and (b) the $\mu^+\mu^-$ mode. Panels (c) and (d) show the sum of the $M_{\pi^+\psi(2S)}$ and $M_{\pi^-\psi(2S)}$ distributions in the $\pi^+\pi^- J/\psi$ and $\mu^+\mu^-$ modes, respectively. The shaded histograms are the backgrounds from the normalized $\psi(2S)$ mass sidebands.

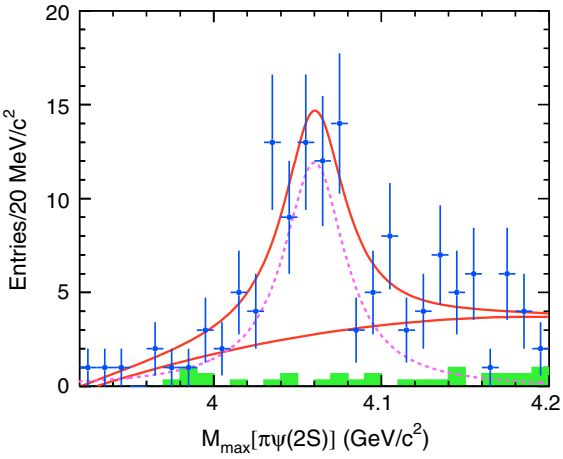

FIG. 13 (color online). The distribution of $M_{\max}(\pi^{\pm}\psi(2S))$ from $Y(4360)$-subsample decays. The points with error bars represent the data; the histogram is from the sidebands and normalized to the signal region; the solid curve is the best fit and the dashed curve is the signal parametrized by a Breit-Wigner function.

$Y(4360)$ or $Y(4660)$ decays. For the $Y(4360)$ subsample, $4.0\ \mathrm{GeV}/c^2 < M_{\pi^+\pi^-\psi(2S)} < 4.5\ \mathrm{GeV}/c^2$ is required; for the $Y(4660)$ subsample, $4.5\ \mathrm{GeV}/c^2 < M_{\pi^+\pi^-\psi(2S)} < 4.9\ \mathrm{GeV}/c^2$ is required.

Figure 12 shows the scatter plots of $M_{\pi^-\psi(2S)}$ versus $M_{\pi^+\psi(2S)}$ and the one-dimensional projections in the $Y(4360)$ subsample. There is an excess evident at around $4.05\ \mathrm{GeV}/c^2$ in the $\pi^{\pm}\psi(2S)$ invariant-mass distributions in both modes. An unbinned maximum-likelihood fit is performed on the distribution of $M_{\max}(\pi^{\pm}\psi(2S))$, the maximum of $M(\pi^+\psi(2S))$ and $M(\pi^-\psi(2S))$, simultaneously with both modes. The excess is parameterized with a Breit-Wigner function and the nonresonant noninterfering background with a second-order polynomial function. The fit yields a mass of $(4060 \pm 3)\ \mathrm{MeV}/c^2$ and a width of (45 ± 11) MeV for the excess, as shown in Fig. 13. Here, the errors are statistical only.

A MC sample for $Y(4360) \to \pi^{\mp} + Z^{\pm}$ and $Z^{\pm} \to \pi^{\pm} + \psi(2S)$ is generated to simulate the excess seen in the data. In the simulation, the mass of $Z^{\pm}$ is $4050\ \mathrm{MeV}/c^2$ and the width is 40 MeV. A fit to the simulated $M_{\max}(\pi^{\pm}\psi(2S))$ distribution yields $M = (4056 \pm 1)\ \mathrm{MeV}/c^2$ and $\Gamma = (40.8 \pm 2.2)$ MeV. The shift in the mass is due to the fact that the reflection of the signal may have a larger $\pi^{\pm}\psi(2S)$ mass than the proper combination, thus biasing $M_{\max}(\pi^{\pm}\psi(2S))$. We shift the measured mass by $\Delta M = -6\ \mathrm{MeV}/c^2$ to account for this effect and assign $1\ \mathrm{MeV}/c^2$ as its systematic error. $\Delta\Gamma = 3.0$ MeV is taken as the systematic error of the measured width.

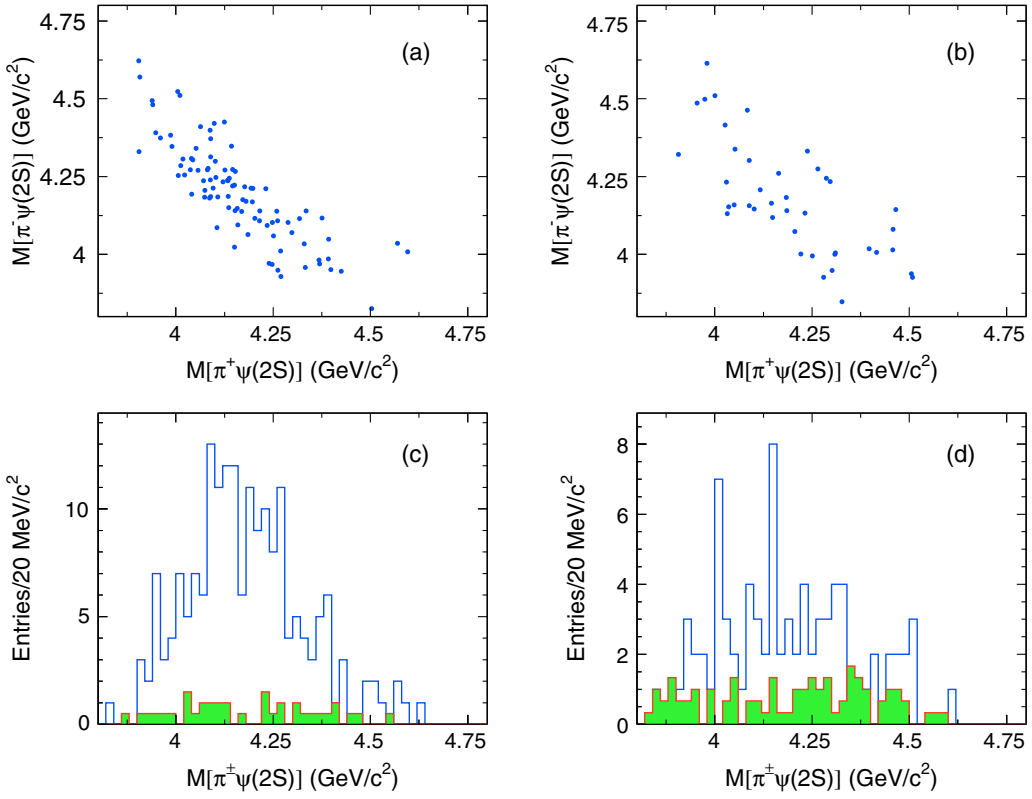

FIG. 14 (color online). The scatter plots of $M_{\pi^-\psi(2S)}$ versus $M_{\pi^+\psi(2S)}$ for the $Y(4660)$ events in the (a) $\pi^+\pi^- J/\psi$ mode and (b) the $\mu^+\mu^-$ mode. Panels (c) and (d) show the sum of the $M_{\pi^+\psi(2S)}$ and $M_{\pi^-\psi(2S)}$ distributions in the $\pi^+\pi^- J/\psi$ and $\mu^+\mu^-$ modes, respectively. The shaded histograms are the backgrounds from the normalized sidebands.

After the bias correction based on MC simulation, we obtain a mass of $(4054 \pm 3(\text{stat}) \pm 1(\text{syst}))$ MeV/c^2 and a width of $(45 \pm 11(\text{stat}) \pm 6(\text{syst}))$ MeV for the $Z^{\pm}$ structure in the $\pi^{\pm}\psi(2S)$ system. The systematic uncertainties from the parametrization of the resonances, the phase-space factor due to the J^P assignment of the structure, the fit range, and the background shape are considered. The lowest statistical significance of the signal is 3.5σ when comparing without the Breit-Wigner component.

Figure 14 shows the scatter plots of $M_{\pi^-\psi(2S)}$ versus $M_{\pi^+\psi(2S)}$ and the one-dimensional projections in the $Y(4660)$ subsample. This subsample is limited in statistics —there is no significant structure in the $\pi^{\pm}\psi(2S)$ system.

VII. SUMMARY

In summary, the $e^+e^- \to \pi^+\pi^-\psi(2S)$ cross section is measured from 4.0 to 5.5 GeV with the full data sample of the Belle experiment using the ISR technique. The parameters of the $Y(4360)$ and $Y(4660)$ resonances are determined; our results agree with and supersede the previous Belle determination [7]. Our results also agree with the *BABAR* measurement [10] but with better precision.

We search for a possible charged charmoniumlike structure in $M_{\pi^{\pm}\psi(2S)}$ distribution. We find an excess at $M_{\pi^{\pm}\psi(2S)} = 4.05$ GeV/c^2 in the $Y(4360)$ decays with a 3.5σ significance. More data from the BESIII [25] and the Belle II [26] experiments will enable a search with improved sensitivity.

ACKNOWLEDGMENTS

We thank the KEKB group for the excellent operation of the accelerator; the KEK cryogenics group for the efficient operation of the solenoid; and the KEK computer group, the National Institute of Informatics, and the PNNL/EMSL computing group for valuable computing and SINET4 network support. We acknowledge support from the Ministry of Education, Culture, Sports, Science, and Technology (MEXT) of Japan, the Japan Society for the Promotion of Science (JSPS), and the Tau-Lepton Physics Research Center of Nagoya University; the Australian Research Council and the Australian Department of Industry, Innovation, Science and Research; Austrian Science Fund under Grants No. P 22742-N16 and No. P 26794-N20; the National Natural Science Foundation of China under Contracts No. 10575109, No. 10775142, No. 10875115, No. 11175187, and No. 11475187; the Chinese Academy of Science Center for Excellence in Particle Physics; the Ministry of Education, Youth and Sports of the Czech Republic under Contract No. LG14034; the Carl Zeiss Foundation, the Deutsche Forschungsgemeinschaft and the VolkswagenStiftung; the Department of Science and Technology of India; the Istituto Nazionale di Fisica Nucleare of Italy; National Research Foundation (NRF) of Korea Grants No. 2011-0029457, No. 2012-0008143, No. 2012R1A1A2008330, No. 2013R1A1A3007772, No. 2014R1A2A2A01005286, No. 2014R1A2A2A01002734, and No. 2014R1A1A2006456; the Basic Research Lab program under NRF Grants No. KRF-2011-0020333 and No. KRF-2011-0021196; Center for Korean J-PARC Users, Grant No. NRF-2013K1A3A7A06056592; the Brain Korea 21-Plus program and the Global Science Experimental Data Hub Center of the Korea Institute of Science and Technology Information; the Polish Ministry of Science and Higher Education and the National Science Center; the Ministry of Education and Science of the Russian Federation and the Russian Foundation for Basic Research; the Slovenian Research Agency; the Basque Foundation for Science (IKERBASQUE) and the Euskal Herriko Unibertsitatea (UPV/EHU) under Program No. UFI 11/55 (Spain); the Swiss National Science Foundation; the National Science Council and the Ministry of Education of Taiwan; and the U.S. Department of Energy and the National Science Foundation. This work is supported by a Grant-in-Aid from MEXT for Science Research in a Priority Area ("New Development of Flavor Physics") and from JSPS for Creative Scientific Research ("Evolution of Tau-lepton Physics").

APPENDIX A: FITS TO $e^+e^- \to \pi^+\pi^-\psi(2S)$ USING $\pi^+\pi^-J/\psi$ MODE ONLY

To compare with the previous measurement from Belle [7], a fit to the $\pi^+\pi^-J/\psi$ mode only is also performed; the fit results are shown in Fig. 15 and Table V. There are differences in the fit results between this measurement and the previous one [7]; this can be explained by the strong

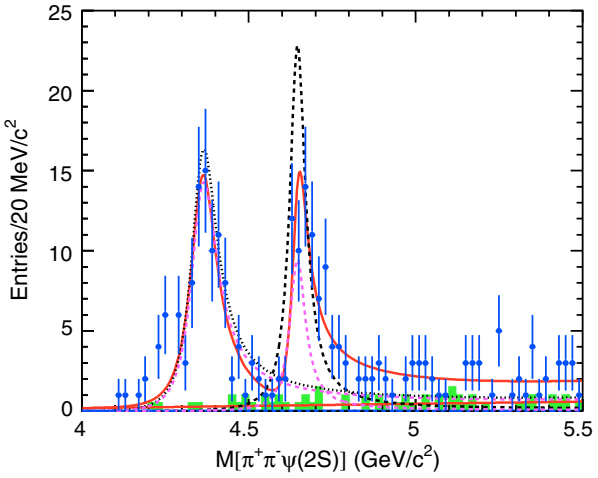

FIG. 15 (color online). The $\pi^+\pi^-\psi(2S)$ invariant-mass distributions and the fit results for the $\pi^+\pi^-J/\psi$ mode only. The details of the plot are the same as those in Fig. 9.

TABLE V. Results of the fits to the $\pi^+\pi^-\psi(2S)$ invariant-mass spectra, using the $\pi^+\pi^- J/\psi$ mode only. The details are the same as those in Table I.

Parameters	Solution I	Solution II
$M_{Y(4360)}$	$4358 \pm 6 \pm 2$	
$\Gamma_{Y(4360)}$	$96 \pm 10 \pm 6$	
$\mathcal{B}[Y(4360) \to \pi^+\pi^-\psi(2S)] \cdot \Gamma^{e^+e^-}_{Y(4360)}$	$9.4 \pm 0.8 \pm 0.7$	$10.8 \pm 0.7 \pm 0.7$
$M_{Y(4660)}$	$4644 \pm 7 \pm 5$	
$\Gamma_{Y(4660)}$	$57 \pm 9 \pm 5$	
$\mathcal{B}[Y(4660) \to \pi^+\pi^-\psi(2S)] \cdot \Gamma^{e^+e^-}_{Y(4660)}$	$3.1 \pm 0.5 \pm 0.4$	$7.6 \pm 1.3 \pm 0.9$
ϕ	$10 \pm 17 \pm 12$	$288 \pm 10 \pm 5$

correlation between the parameters. For example, the correlation coefficient between $M_{Y(4660)}$ and ϕ is 0.86 for one solution (or −0.76 for the other solution) in the fit shown in Tables I and II.

The fit to the $\pi^+\pi^- J/\psi$ mode only with the coherent sum of $Y(4260)$, $Y(4360)$, and $Y(4660)$ is shown in Fig. 16 and Table VI. The statistical significance of the $Y(4260)$ is 2.8σ in this fit.

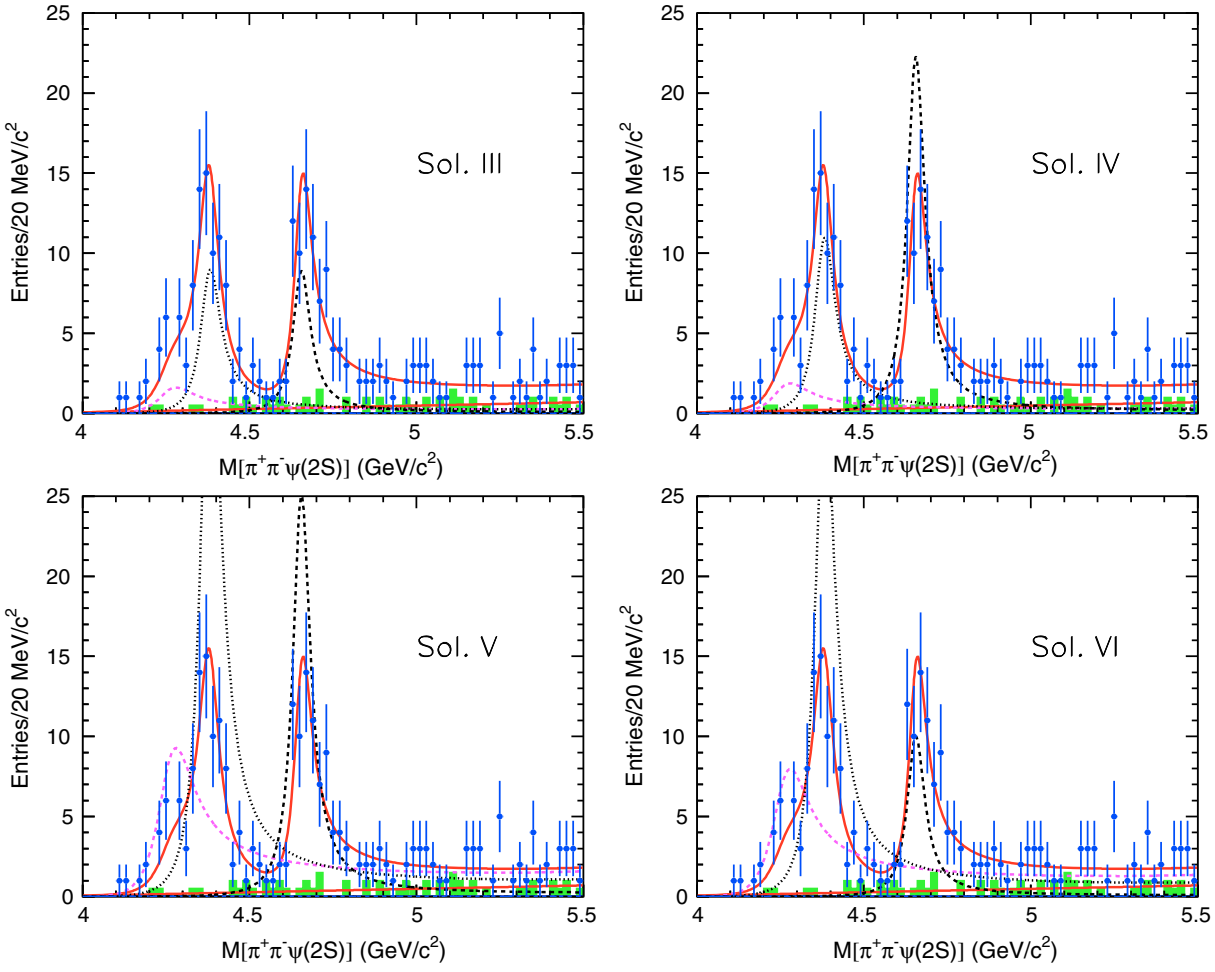

FIG. 16 (color online). The four solutions from the fit to the $\pi^+\pi^-\psi(2S)$ invariant-mass spectra with the $Y(4260)$ included but for the $\pi^+\pi^- J/\psi$ mode only. The details are the same as those in Fig. 10.

TABLE VI. Results of the fits to the $\pi^+\pi^-\psi(2S)$ invariant-mass spectra in $\pi^+\pi^- J/\psi$ mode only using three resonances, the $Y(4260)$, $Y(4360)$, and $Y(4660)$. The details are the same as those from Table III.

Parameters	Solution III	Solution IV	Solution V	Solution VI
$M_{Y(4260)}$		4259 (fixed)		
$\Gamma_{Y(4260)}$		134 (fixed)		
$\mathcal{B}[Y(4260)\to\pi^+\pi^-\psi(2S)]\cdot\Gamma^{e^+e^-}_{Y(4260)}$	$1.6\pm0.6\pm0.4$	$1.8\pm0.8\pm0.6$	$9.1\pm1.2\pm0.7$	$7.8\pm1.1\pm0.8$
$M_{Y(4360)}$		$4378\pm9\pm6$		
$\Gamma_{Y(4360)}$		$74\pm14\pm3$		
$\mathcal{B}[Y(4360)\to\pi^+\pi^-\psi(2S)]\cdot\Gamma^{e^+e^-}_{Y(4360)}$	$4.5\pm1.0\pm0.4$	$5.5\pm1.4\pm0.6$	$19.1\pm2.8\pm1.1$	$15.7\pm2.3\pm1.6$
$M_{Y(4660)}$		$4654\pm7\pm6$		
$\Gamma_{Y(4660)}$		$65\pm10\pm3$		
$\mathcal{B}[Y(4660)\to\pi^+\pi^-\psi(2S)]\cdot\Gamma^{e^+e^-}_{Y(4660)}$	$3.3\pm0.6\pm0.3$	$8.3\pm1.0\pm0.9$	$9.3\pm1.2\pm1.2$	$3.7\pm0.7\pm0.5$
ϕ_1	$282\pm25\pm24$	$270\pm27\pm28$	$130\pm5\pm3$	$142\pm6\pm7$
ϕ_2	$359\pm19\pm3$	$243\pm17\pm20$	$337\pm10\pm7$	$93\pm25\pm17$

APPENDIX B: CROSS SECTION OF $e^+e^-\to\pi^+\pi^-\psi(2S)$

The cross sections of $e^+e^-\to\pi^+\pi^-\psi(2S)$ in the full solid angle are shown in Table VII. What we list here is the averaged cross section over a 20 MeV bin centered at $E_{\rm cm}$ listed in the table.

TABLE VII. Measured $e^+e^-\to\pi^+\pi^-\psi(2S)$ cross section for center of mass energy ($E_{\rm cm}$) from 4.0 to 5.5 GeV. The errors are the sums of statistical errors of signal and background events and the systematic errors.

$E_{\rm cm}$ (GeV)	Cross section (pb)	$E_{\rm cm}$ (GeV)	Cross section (pb)	$E_{\rm cm}$ (GeV)	Cross section (pb)
4.01	-19.1 ± 31.4	4.51	18.4 ± 8.4	5.01	3.7 ± 4.6
4.03	-15.3 ± 24.9	4.53	14.9 ± 7.6	5.03	10.1 ± 5.3
4.05	-12.8 ± 20.7	4.55	5.5 ± 5.2	5.05	5.8 ± 4.3
4.07	-11.0 ± 17.8	4.57	-0.5 ± 4.6	5.07	3.6 ± 3.6
4.09	-9.7 ± 15.7	4.59	8.2 ± 5.8	5.09	3.5 ± 3.6
4.11	-0.5 ± 12.9	4.61	10.9 ± 6.4	5.11	-2.6 ± 3.5
4.13	-0.5 ± 11.7	4.63	33.0 ± 10.2	5.13	-2.6 ± 3.4
4.15	-0.5 ± 10.7	4.65	29.7 ± 9.6	5.15	7.4 ± 4.5
4.17	5.9 ± 9.0	4.67	37.3 ± 10.6	5.17	7.3 ± 4.4
4.19	5.4 ± 11.0	4.69	34.1 ± 10.1	5.19	5.2 ± 3.9
4.21	-6.0 ± 9.4	4.71	20.4 ± 7.9	5.21	-0.6 ± 3.0
4.23	20.4 ± 11.7	4.73	22.7 ± 8.2	5.23	5.0 ± 3.8
4.25	29.2 ± 13.2	4.75	9.6 ± 5.7	5.25	10.5 ± 5.0
4.27	8.9 ± 9.9	4.77	14.5 ± 6.7	5.27	-0.6 ± 2.9
4.29	26.5 ± 12.0	4.79	9.4 ± 5.6	5.29	1.2 ± 2.6
4.31	25.3 ± 11.4	4.81	4.3 ± 5.2	5.31	6.5 ± 4.0
4.33	61.5 ± 16.8	4.83	1.9 ± 4.5	5.33	-0.6 ± 2.7
4.35	67.1 ± 17.2	4.85	6.6 ± 4.8	5.35	4.6 ± 4.0
4.37	80.1 ± 18.4	4.87	6.5 ± 4.7	5.37	-0.6 ± 2.6
4.39	40.4 ± 13.0	4.89	11.1 ± 5.7	5.39	2.7 ± 2.9
4.41	42.7 ± 13.1	4.91	6.3 ± 4.6	5.41	-0.6 ± 2.6
4.43	31.0 ± 11.2	4.93	4.0 ± 4.0	5.43	2.6 ± 3.4
4.45	9.7 ± 6.8	4.95	-2.8 ± 3.8	5.45	4.1 ± 3.2
4.47	12.8 ± 7.4	4.97	1.6 ± 4.1	5.47	5.6 ± 3.5
4.49	6.0 ± 5.6	4.99	6.0 ± 4.4	5.49	-0.6 ± 2.4

[1] N. Brambilla *et al.*, Eur. Phys. J. C **71**, 1534 (2011); **74**, 2981 (2014).
[2] C.-Z. Yuan, Int. J. Mod. Phys. A **29**, 1430046 (2014).
[3] B. Aubert *et al.* (*BABAR* Collaboration), Phys. Rev. Lett. **95**, 142001 (2005).
[4] Q. He *et al.* (CLEO Collaboration), Phys. Rev. D **74**, 091104(R) (2006).
[5] C. Z. Yuan *et al.* (Belle Collaboration), Phys. Rev. Lett. **99**, 182004 (2007).
[6] B. Aubert *et al.* (*BABAR* Collaboration), Phys. Rev. Lett. **98**, 212001 (2007).
[7] X. L. Wang *et al.* (Belle Collaboration), Phys. Rev. Lett. **99**, 142002 (2007).
[8] J. P. Lees *et al.* (*BABAR* Collaboration), Phys. Rev. D **86**, 051102(R) (2012).
[9] Z. Q. Liu *et al.* (Belle Collaboration), Phys. Rev. Lett. **110**, 252002 (2013).
[10] B. Aubert *et al.* (*BABAR* Collaboration), Phys. Rev. D **89**, 111103 (2014).
[11] X. L. Wang *et al.* (Belle Collaboration), Phys. Rev. D **87**, 051101(R) (2013).
[12] M. Ablikim *et al.* (BESIII Collaboration), Phys. Rev. Lett. **110**, 252001 (2013).
[13] M. Ablikim *et al.* (BESIII Collaboration), Phys. Rev. Lett. **111**, 242001 (2013).
[14] A. Abashian *et al.* (Belle Collaboration), Nucl. Instrum. Methods Phys. Res., Sect. A **479**, 117 (2002); J. Brodzicka *et al.*, Prog. Theor. Exp. Phys. **2012**, 04D001 (2012).
[15] S. Kurokawa and E. Kikutani, Nucl. Instrum. Methods Phys. Res., Sect. A **499**, 1 (2003), and other papers included in this volume; T. Abe *et al.*, Prog. Theor. Exp. Phys. **2013**, 03A001 (2013), and following articles up to 03A011.
[16] R. Brun *et al.*, CERN Report No. CERN DD/EE/84-1, 1984.
[17] G. Rodrigo, H. Czyż, J. H. Kühn, and M. Szopa, Eur. Phys. J. C **24**, 71 (2002); S. Actis *et al.*, Eur. Phys. J. C **66**, 585 (2010).
[18] E. Nakano, Nucl. Instrum. Methods Phys. Res., Sect. A **494**, 402 (2002).
[19] K. Hanagaki, H. Kakuno, H. Ikeda, T. Iijima, and T. Tsukamoto, Nucl. Instrum. Methods Phys. Res., Sect. A **485**, 490 (2002).
[20] A. Abashian *et al.*, Nucl. Instrum. Methods Phys. Res., Sect. A **491**, 69 (2002).
[21] J. Beringer *et al.* (Particle Data Group), Phys. Rev. D **86**, 010001 (2012).
[22] $M_{\pi^+\pi^- J/\psi} = M_{\pi^+\pi^-\ell^+\ell^-} - M_{\ell^+\ell^-} + m_{J/\psi}$ is used to cancel the lepton-pair mass resolution in the $\pi^+\pi^- J/\psi$ invariant-mass spectrum; here, $m_{J/\psi}$ is the nominal mass of J/ψ [21].
[23] $M_{\pi^+\pi^-\psi(2S)} = M_{\pi^+\pi^-\pi^+\pi^-\ell^+\ell^-} - M_{\pi^+\pi^-\ell^+\ell^-} + m_{\psi(2S)}$ for the $\pi^+\pi^- J/\psi$ mode and $M_{\pi^+\pi^-\psi(2S)} = M_{\pi^+\pi^-\mu^+\mu^-} - M_{\mu^+\mu^-} + m_{\psi(2S)}$ for the $\mu^+\mu^-$ mode, where $m_{\psi(2S)}$ is the $\psi(2S)$ nominal mass [21].
[24] E. A. Kuraev and V. S. Fadin, Yad. Fiz. **41**, 733 (1985) [Sov. J. Nucl. Phys. **41**, 466 (1985)].
[25] M. Ablikim *et al.* (BESIII Collaboration), Nucl. Instrum. Methods Phys. Res., Sect. A **614**, 345 (2010).
[26] T. Abe *et al.* (Belle II Collaboration), arXiv:1011.0352.